

# Numerical Analysis of Active Cascade Flutter Control with Smart Structure

Junichi Kazawa and Toshinori Watanabe

Department of Aeronautics and Astronautics  
The University of Tokyo

7-3-1 Hongo, Bunkyo-ku, Tokyo 113-8656, JAPAN

Phone: +81-3-5841-6624, FAX: +81-3-5841-6622, E-mail: kazawa@aero.t.u-tokyo.ac.jp

## ABSTRACT

A numerical method in which the flow-structure coupling was taken into account was newly developed to study the possibility of active cascade flutter control by the application of smart structure. Numerical analyses were performed under transonic flow condition with passage shock waves where the unsteady aerodynamic force induced by the shock oscillation was dominant for instability of blade vibration. In the present study, the trailing edge of a blade was actively oscillated to control the unsteady aerodynamic force through the change in the behavior of shock waves around an oscillating blade. From the numerical results, the effective alleviation or suppression of blade vibration was obtained in the case of unstable oscillation if the phase difference between the trailing edge oscillation and blade displacement was adequately selected. When the control was effective, the unsteady aerodynamic force acted on blades was changed from exciting to damping due to the phase change of unsteady aerodynamic force. The phase change should be caused by the change in the back pressure of a flow channel, which was probably introduced by the active oscillation of trailing edge with a proper phase angle. The active oscillation can be realized with, for instance, a piezo-electric device.

## NOMENCLATURE

A= Blade Vibration Amplitude  
C= Chord Length  
 $C_f$ = Unsteady Aerodynamic Force on Blade  
 $C_n$ = Influence Coefficient  
D= Structural Damping of Blade  
E= Total Energy of Blade  
K= Blade Stiffness  
L= Lift acting on Blade  
M= Blade Mass  
N= Number of Flow Channels or Blades  
U= Velocity  
V= Blade Oscillation Velocity  
d,  $d_0$  = Distance between Grid Points, Fig.4  
 $f$ = Blade Frequency  
h= Blade Displacement  
 $k$ = Reduced Frequency =  $2\pi f C/U$   
p= Static Pressure  
u= Axial Velocity  
 $\rho$ = Density  
 $\sigma$ = Inter Blade Phase Angle  
 $\omega$ = Natural Angular Frequency

subscripts

0 = Inlet Condition

1 = Outlet Condition

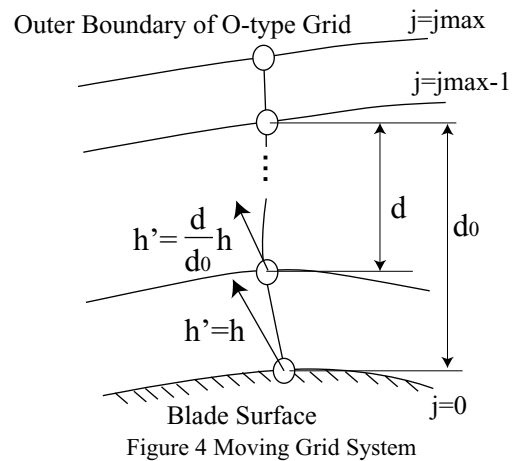
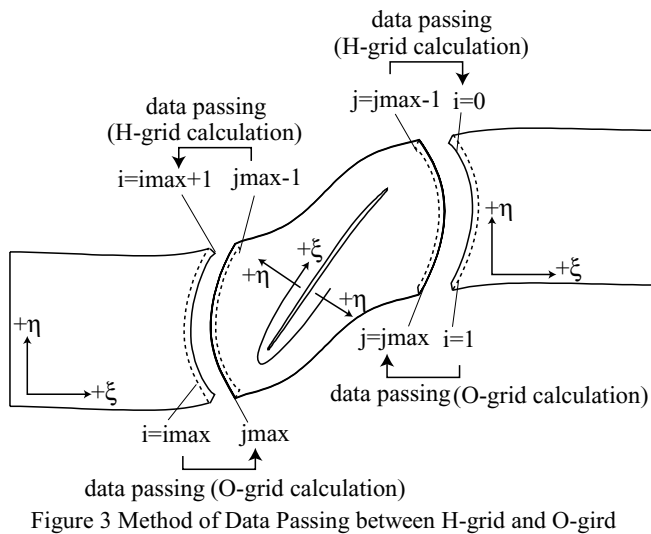
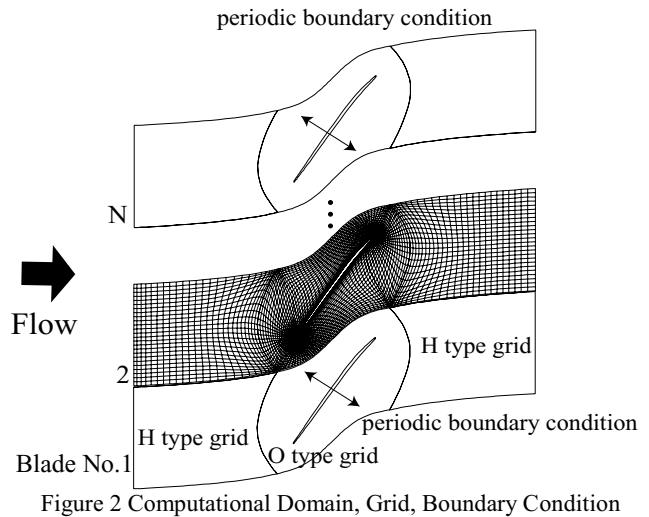
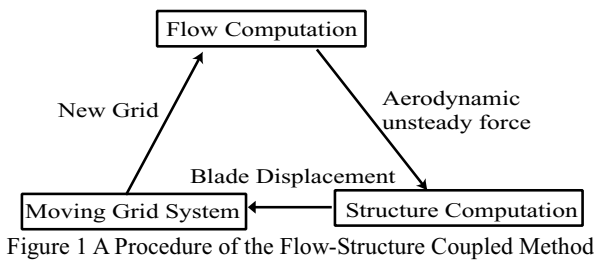
## INTRODUCTION

Toward intelligent gas turbine technology in the near future, the control of unsteady aerodynamic and aeroelastic phenomena in compressors is one of the key technologies from the viewpoint of ultra-high efficiency and reliability. Active control techniques of surge and rotating stall have widely been studied in the last decade and fruitful achievements have been obtained [1]. Concerning the cascade flutter problem, some active control techniques have also been reported so far. For example, the acoustic waves were introduced into the cascade flow field to suppress the exciting force on the blades [2], or the acoustic impedance on the casing wall of a compressor was actively controlled to reduce the exciting energy of the oscillating blade [3].

On the other hand, the study of "smart materials" or "smart structures" has been rapidly advanced in the research field of structures and materials. The smart materials can deform themselves reacting to electric signals. Active control techniques by the application of the smart structures have been proposed for the vibration control of aircraft wing, flap or fuselage panel [4]. The similar technique seems to be applicable to the suppression of cascade flutter, and effective and reliable control method is expected, since such material can directly change the structural characteristics of vibrating materials or can give flexible deformation of the blades.

The authors numerically studied the possibility of active control of cascade flutter with an intension of smart structure application [5]. A numerical analysis method with flow-structure coupling was developed to capture the flutter phenomena and to analyze control techniques. From the results by the developed method so far, the well-known flutter suppression by mistuning effect could properly be simulated in the subsonic flow condition. In a transonic cascade flow with a passage shock wave, the unsteady aerodynamic force on the blade surface was induced mainly by the passage shock oscillation, which force was dominant for blade vibration instability. The numerical analysis in such a situation showed that the increase in blade displacement could be suppressed by changing the movement direction of the oscillating blade.

In the present study, more effective and realistic method of cascade flutter suppression was sought in the transonic flow condition. The method of active trailing edge oscillation was eventually adopted and proposed in the study. In the control method, the blade trailing edge was actively oscillated to control the unsteady aerodynamic force induced by the passage shock movement due to blade oscillation. The trailing edge oscillation can



be realized by piezo-electric device mounted on the blade surface. The effectiveness and the mechanism of the control method were studied by the developed flow-structure coupled method.

## NUMERICAL METHOD

### Flow-Structure Coupling

Figure 1 shows the procedure of the flow-structure coupled method [5]. The developed numerical method is based on the two-dimensional non-linear Euler equation for flow computation, coupled with a dynamic structural model equation of blades in one-degree of freedom. At the first step, the flow computation is performed to obtain the unsteady aerodynamic force acting on all blades. The obtained aerodynamic force is introduced into the structural computation at the next step in which the equation of motion of the blade is solved for obtaining the blade displacement. Then, the computed blade displacement is used for generation of the new grid coordinates in the following time step of flow computation.

### Flow Computation

Two-dimensional non-linear Euler equation is solved through a second order upwind TVD scheme. LU-ADI factorization algorithm [6] is used as the time- marching scheme.

Figure 2 shows computational domain, grid, and boundary conditions. O-grid was adopted around blades to achieve good orthogonality, and H-grid was generated in upstream and

downstream regions in order to place the inlet and outlet boundary far enough from the blade leading and trailing edges.

Figure 3 shows the method of data passing with high accuracy between H-grid and O-grid systems. When the computation in the H-grid part is performed, the data of physical properties at  $j=j_{\max}-1$  in the O-grid are substituted for those at  $i=i_{\max}+1$  in the H-grid. On the other hand, all physical amounts at  $i=i_{\max}$  in the H-grid part are substituted for those at  $j=j_{\max}$  in the O-grid. The number of the H-grid points is 21 both in the streamwise and pitchwise directions, while the number of O-grid points is 141 round the blade and 31 in the direction away from the blade surface. Periodic boundary conditions were imposed on the upper and lower sides of the computational domain, that is, physical values at the lower boundary of No.1 flow region and those at the upper boundary of No.N flow region were set to be same, and quasi-1D non-reflecting boundary condition with Riemann invariant was used on the inlet boundary to prevent the reflection of the wave induced by the blade vibration. At the inlet boundary, total pressure and total temperature were fixed, and rotational speed (tangential velocity) was also fixed. Static pressure was specified at the outlet boundary, and the blade surfaces were treated as slip boundaries.

Figure 4 shows the outline of grid moving system to simulate the blade vibration. The O-grid is moved according to the blade oscillation, while the H-grid is set stationary. The grid points at the outer boundary of the O-grid system,  $j=j_{\max}$  and  $j_{\max}-1$ , are fixed, and the inner grid points are moved by the following displacement  $h'$ ;

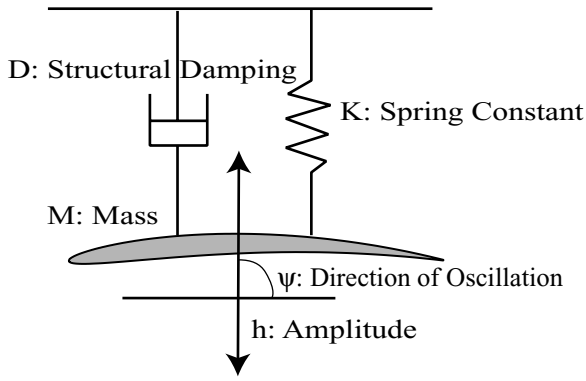


Figure 5 Structural Model

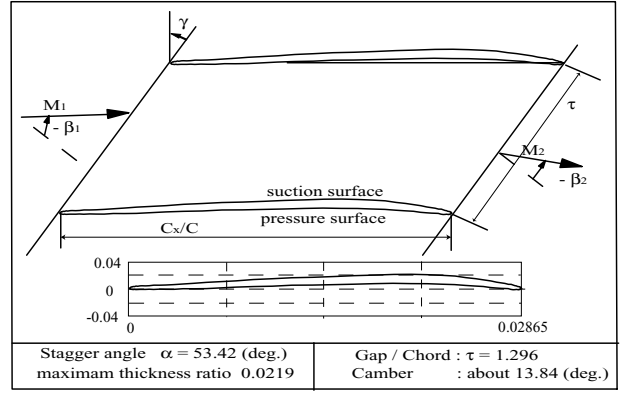


Figure 6 Cascade Model  
(Tip Section of NASA Quiet Fan B)

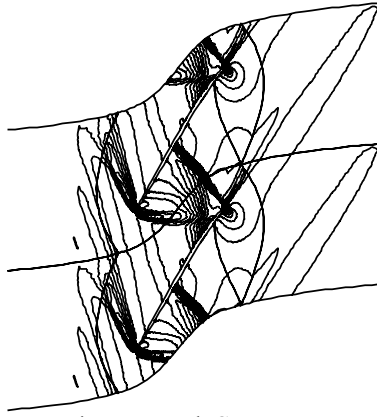


Figure 7 Mach Contours  
( $M_0=1.25$ ,  $p_1/p_0=1.7$ )

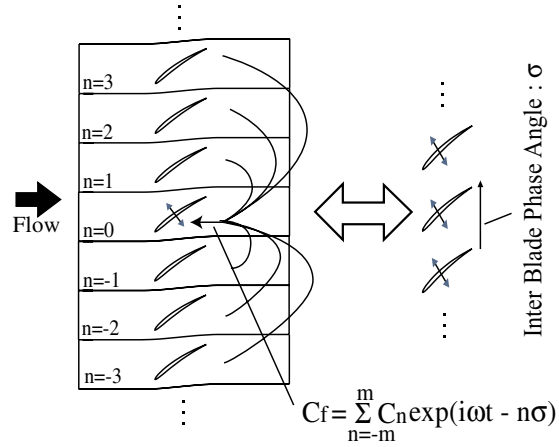


Figure 8 Concept of Influence Coefficient Method

$$h' = h \frac{d}{d_0} \quad (1)$$

$$M \frac{d^2 h}{dt^2} + D \frac{dh}{dt} + Kh = L \quad (3)$$

where,  $h$  is the blade displacement,  $d$  is the distance of a grid point measured from the  $j=j_{\max}-1$  boundary, and  $d_0$  is the distance between the blade surface and the grid point at  $j=j_{\max}-1$ . The displacement is thus inversely proportional to the distance from the blade surface.

The number of flow channels,  $N$ , can be arbitrarily selected in the computation, and the inter blade phase angles of  $360$  (deg)  $\times n/N$  ( $n=1, 2, \dots, N$ ) can be existed in  $N$  flow channels.

The aerodynamic force acting on a blade,  $L$ , is obtained by the integration of blade surface pressure. The unsteady component of the aerodynamic force,  $L_{unsteady}$ , is calculated by

$$L_{unsteady} = L - L_{steady} \quad (2)$$

where  $L_{steady}$  is the steady aerodynamic force computed in the case without blade vibration.

The verification of the flow simulation is presented in Ref. [5]

### Structure Computation

Figure 5 shows the structural model of blades for a translational (bending) mode. The direction of blade movement, indicated by the angle  $\Psi$ , can be arbitrarily selected. It is well known that the direction angle,  $\psi$ , is a quite important parameter for vibration characteristics of blades. The vibration equation of the blade model;

is solved through the Runge-Kutta-Gill scheme. The lift force on the blade,  $L$ , calculated in the flow computation is introduced into the right hand side of Eq. (3) to achieve flow-structure coupling. To focus on the aerodynamic damping effect in the flow-structure coupled situation, the structural damping,  $D$ , was neglected in the present analysis. The stiffness parameter,  $K=M\omega^2$ , was set to be  $2.45 \times 10^5$  (N/m). This value of  $K$  is not far from that of realistic cascades. The mass ratio of the blade,  $m_r = M/\rho\pi(C/2)^2$ , was about 200, a typical value for a compressor blade.

### ACTIVE FLUTTER SUPPRESSION IN TRANSONIC FLOW CONDITION

#### Cascade Model

The tip section of the Quiet Fan B in NASA Quiet Engine Program [7], shown in Fig.6, was adopted as a typical transonic cascade model. The inlet Mach number was 1.25, and the static pressure ratio  $p_1/p_0$  was 1.7.

Figure 7 shows the computed steady Mach contour diagram. A passage shock generated at the trailing edge of each blade can be clearly seen in the flow channel. The passage shock is oscillated due to the blade vibration, and the oscillation accordingly induces unsteady aerodynamic force on the blade surface. Concerning vibration instability of this cascade, the shock oscillation is known to be the most influential factor[8].

### Vibration Instability

It is necessary to find the conditions under which the blade vibration becomes unstable for simulating cascade flutter phenomenon by the flow-structure coupled method. The condition was obtained from the analytical results by the Influence Coefficient Method [9]. Figure 8 describes the concept of the method. The reference blade No.0 is oscillated, while the other blades are set stationary. In this situation, the unsteady aerodynamic force acts on No.n blade,  $C_n$ , is obtained through the following integration of the unsteady surface pressure,

$$C_n = \oint_{\text{bladesurface}} p \, dl = L \quad (4)$$

The unsteady aerodynamic force of each blade is linearly superposed as Eq. (5) to obtain the unsteady aerodynamic force when all blades are oscillating with an arbitrary inter blade phase angle.

$$C_f = \frac{\sum_{n=-m}^m C_n \exp(i\omega t - n\sigma)}{\frac{1}{2} \rho_0 U_0^2} \quad (5)$$

where,  $n$  is the blade number,  $C_f$  is the unsteady aerodynamic force in the case when all blades are oscillating with an inter blade phase angle of  $\sigma$ , and  $C_n$  is the influence coefficient of blade No. $n$ .

In the present analysis, five flow channels were used ( $m=2$ ), since the influence coefficients of No. 3 blade and No. -3 blade were negligibly small. Flow condition is the same as those in the results of Fig.7, and oscillation direction,  $\Psi$ , was 120 degrees.

Figure 9 shows the calculated unsteady aerodynamic work on a blade against the inter blade phase angle. The reduced frequency is 0.084. The unsteady aerodynamic work,  $W$ , is calculated by Eq. (6),

$$W = \frac{\oint_{\text{cycle}} \frac{\partial h}{\partial t} C_f dt}{A} \quad (6)$$

where,  $C_f$  is the unsteady aerodynamic force and  $A$  is the amplitude of blade oscillation. Blade vibration is unstable in the case when the

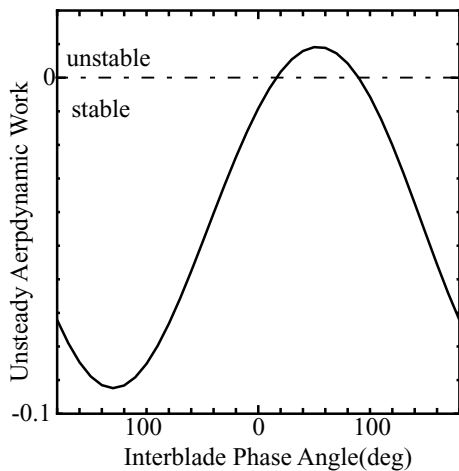


Figure 9 Unsteady Aerodynamic Work

aerodynamic work is positive. In Fig.9, the aerodynamic work is found to be positive around 90 degrees of the inter blade phase angle. The reduced frequency of 0.084 is representatively used here for analysis of unstable vibration.

Figure 10 shows the unsteady aerodynamic work distribution on blade surface when all blades are forced to oscillate with 90 degrees of inter blade phase angle, that is, the case of unstable blade vibration. The positive value of the unsteady aerodynamic work means that the unsteady aerodynamic force is acting on a blade as an exciting force. In the pressure surface result, a peak can be seen at around 50 % of chord. From the result of Fig.7, this is the point where passage shock wave reflects on the pressure surface. The peak hence indicates the unsteady aerodynamic work induced by the movement of the passage shock. At 90% of chord length in the suction surface results, there also exists a positive peak. An oblique shock from the leading edge of the adjacent blade impinges here as shown in Fig.7, and the oscillation of the oblique shock must induce the positive unsteady aerodynamic work. From the results shown in Fig.10, it can be concluded that the positive aerodynamic work at 50% chord position on the pressure surface dominates the unstable blade oscillation in the present condition.

### Flutter Simulation in Transonic Flow Condition

The occurrence of cascade flutter was simulated for the adopted cascade model by the developed flow-structure coupled method. The configuration of four flow channels was used for simulating the unstable situation with the inter blade phase angle of 90 degrees. Reduced frequency was 0.084 and  $\Psi=120$  deg. Figure 11 shows computed time histories of the blade displacement and the unsteady aerodynamic force. All blades were set stationary in the initial situation, and an axial velocity disturbance,  $u$ , was given as the following Eq. (7) at the inlet boundary during one period of blade vibration until the time  $t_s$  indicated in Fig.11.

$$u = u_0 (1 + 0.05 \sin(d_j \pi / X)) \quad (7)$$

where,  $d_j$  is the distance from the point S in Fig.11, and  $X$  is the length of the inlet of flow region. It is clearly shown in the result that the blade displacement increases with time after the time  $t_s$ . It is thus verified that the present numerical method adequately simulated the instability of blade vibration in the transonic flow field.

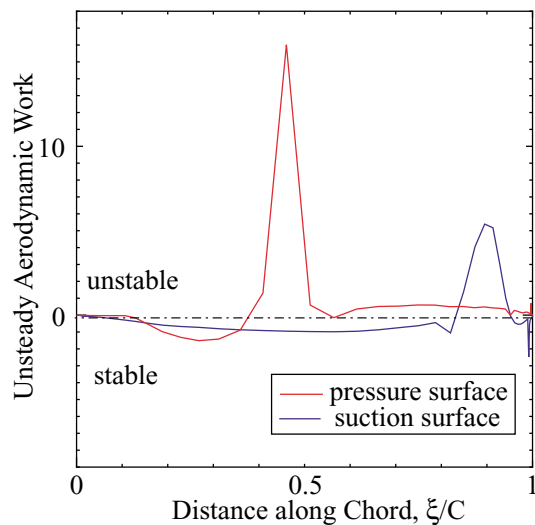


Figure10 Unsteady Aerodynamic Work Distribution on Blade Surface

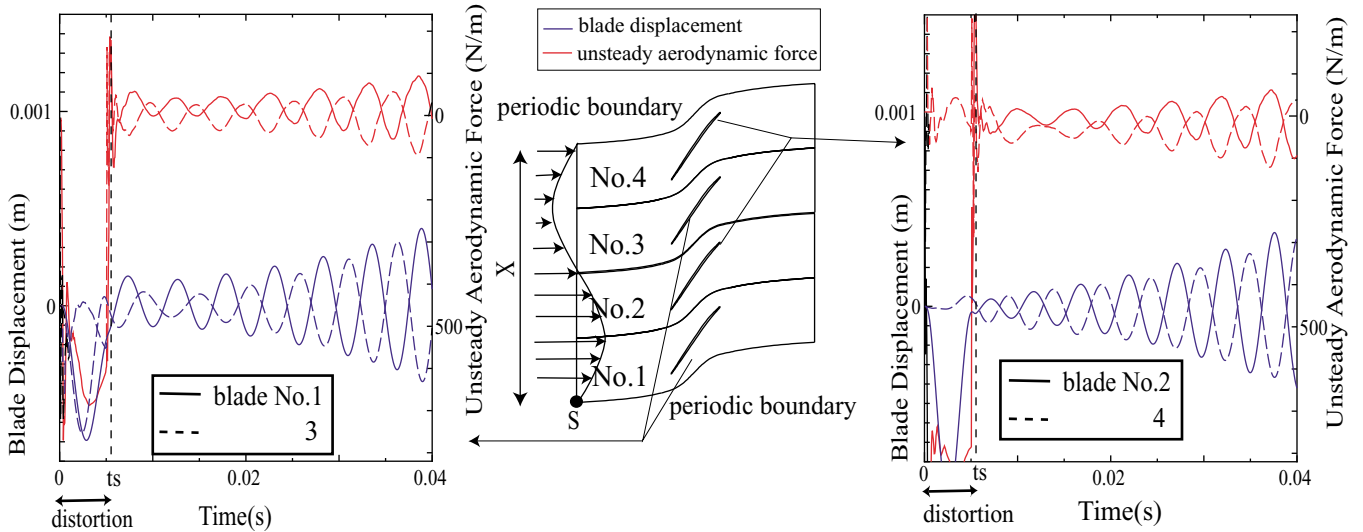


Figure 11 Time History of the Blade Displacement and the Unsteady Aerodynamic Force (unstable case)

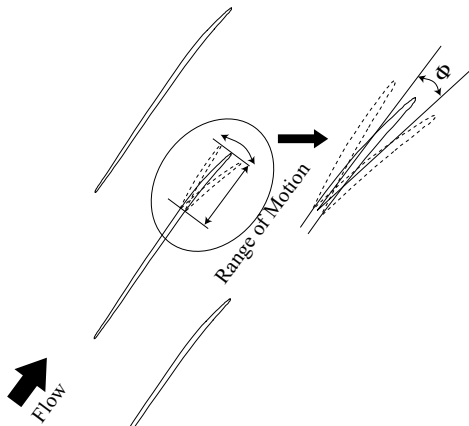


Figure 12 Trailing Edge Oscillation

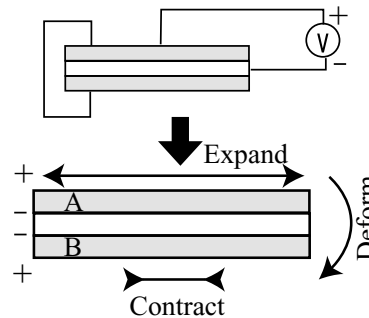


Figure 13 Piezo-Electric Device

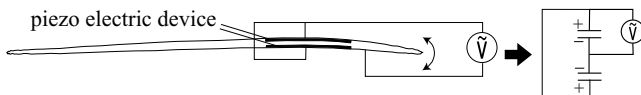


Figure 14 Trailing Edge Oscillation by Piezo-Electric Device

### **Control Method of Trailing Edge Oscillation**

From the results shown in Fig.10, the movement of the passage shock was revealed dominant for the vibration instability of the present cascade. An effective suppression of cascade flutter may therefore be realized if the movement of the passage shock is properly controlled. Such control on the shock movement should be possible through a control of back pressure of the cascade flow passage, and one possible way for the control is to make the trailing edge of a blade vibrate like a flap.

Figure 12 illustrates the method of trailing edge oscillation adopted in the present study. As shown in Fig.12, the flapping oscillation region extends about 30% chord length from the trailing edge and the angular displacement of the oscillation is  $\Phi$ . For example, an active vibration of the trailing edge can be realized by piezo-electric device.

Figure 13 shows the motion mechanism of piezo-electric device. The piezo-electric device on upper surface (A) is expanded and, simultaneously, the lower surface one (B) is contracted when the electric signal is given as in Fig.13. The flat plate is accordingly deformed downward.

Figure 14 shows the idea of trailing edge oscillation using piezo-electric device. Piezo-electric devices are glued on the blade and make an electric circuit as shown in Fig.14. When an AC voltage is provided on the device, the blade section on which the device is glued on is oscillated.

A pilot study of the vibration system showed that the trailing edge oscillation could be realized with the piezo-electric device.

### **Analysis of Active Flutter Suppression by Trailing Edge Oscillation**

To investigate the effect of trailing edge oscillation, the case that all blades were forced to oscillate was analyzed first. Since the frequency of blade oscillation and its amplitude can be specified in this analysis, the fundamental knowledge of the influence by the trailing edge oscillation can be obtained, though the flow and structure analyses are not coupled yet. Based on the results in Fig.9, the inter blade phase angle is fixed to be 90 degrees to simulate the unstable situation of the blade vibration. The phase difference between blade vibration and trailing edge oscillation is important because static pressure on the oscillation region of the blade fluctuates in response to the trailing edge vibration. Hence, the analysis was performed for four cases in which the phase angle of trailing edge oscillation advanced by 0, 90, 180, and 270 degrees compared with that of blade vibration. Since 90 degrees phase advance was revealed most effective for flutter suppression from

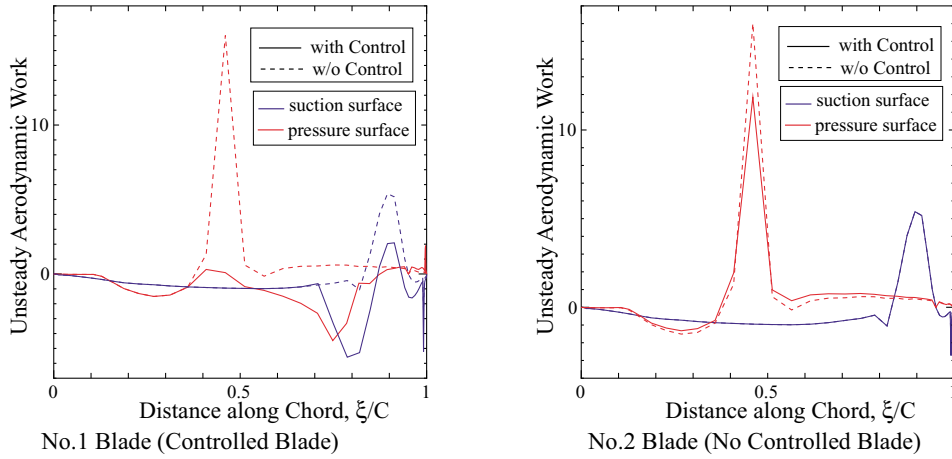


Figure 15 Unsteady Aerodynamic Work Distribution

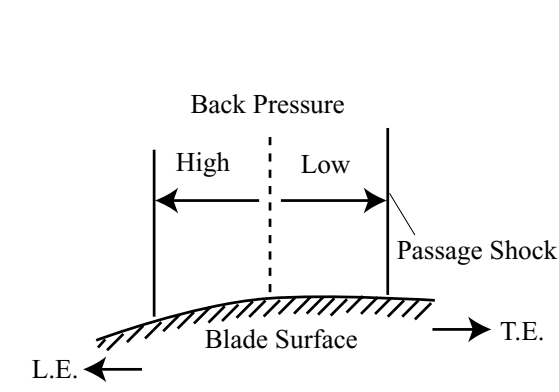


Figure 16 Schematic View of Passage Shock Movement

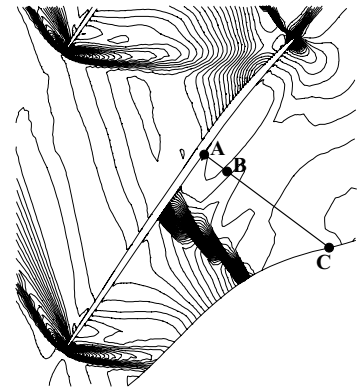


Figure 17 Observation Points of Pressure Data

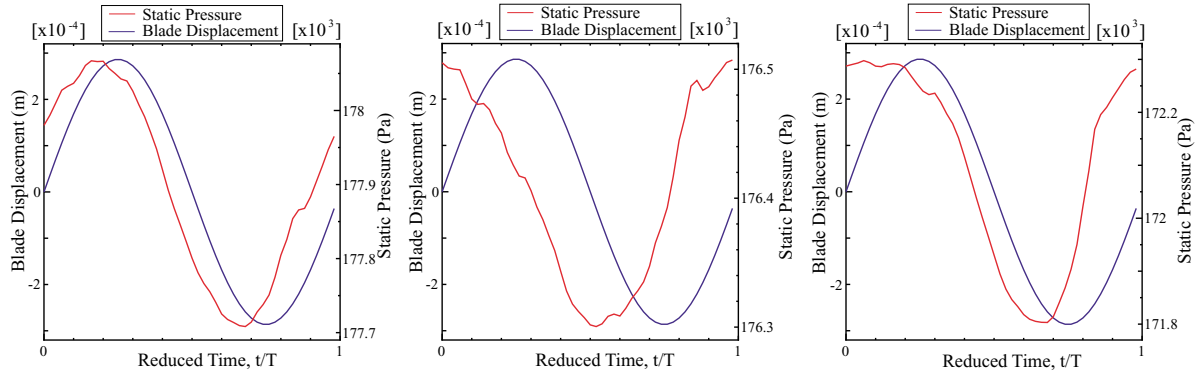


Figure 18 Time History of Static Pressure and Blade Displacement of Blade (without Control) (Left: Point A, Center: Point B, Right: Point C)

the computed result, this case is reported here. The blade on which the trailing edge oscillation is given is called “controlled blade”, while the blade without trailing edge oscillation is called “non-controlled blade”. Four flow channels were used to simulate the inter blade phase angle of 90 degrees. The reduced frequency of the blade oscillation was 0.084 and  $\Phi$  was 1 degree. No.1 and No.3 blades were controlled blades, and No.2 and No.4 blades were non-controlled blades, respectively.

Figure 15 shows unsteady aerodynamic work distributions on the No.1 blade (controlled blade) and No.2 blade (non-controlled blade) surfaces. The results of the case in which no blade is controlled (w/o Control) are also shown for comparison. As shown in Fig.15, the unsteady aerodynamic work around 50% chord

position was drastically changed in the case with control. The peak around 50% chord is diminished by the trailing edge control on the controlled blade. On the non-controlled blade, the height of the peak is decreased by the control. The oscillatory movement of the passage shock was changed by the trailing edge control because the peak of the unsteady work was mostly induced by the shock wave oscillation.

Figure 16 schematically shows the mechanism of the passage shock movement when the back pressure fluctuates. If the back pressure is higher than that of the steady flow field, the passage shock moves to the direction of leading edge and the unsteady aerodynamic force around passage shock acts on the blade in the upward direction. When the back pressure is low, the situation is

contrary.

Since the change in shock wave movement is mainly caused by

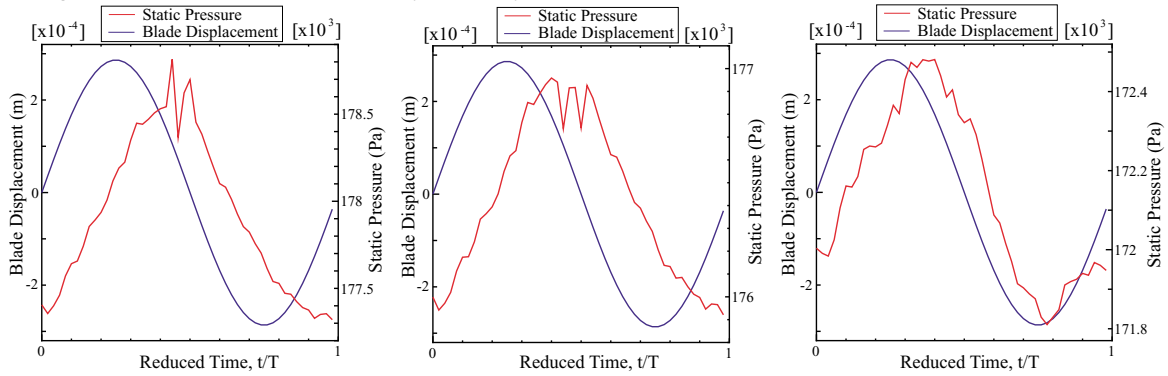


Figure 19 Time History of Static Pressure and Blade Displacement of Controlled Blade (with Control)

(Left: Point A, Center: Point B, Right: Point C)

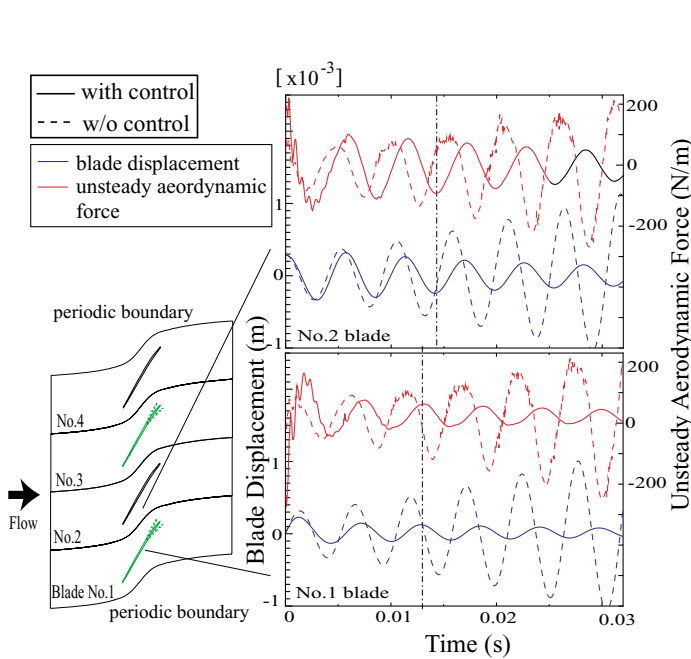


Figure 20 Time History of Blade Displacement and Unsteady Aerodynamic Force

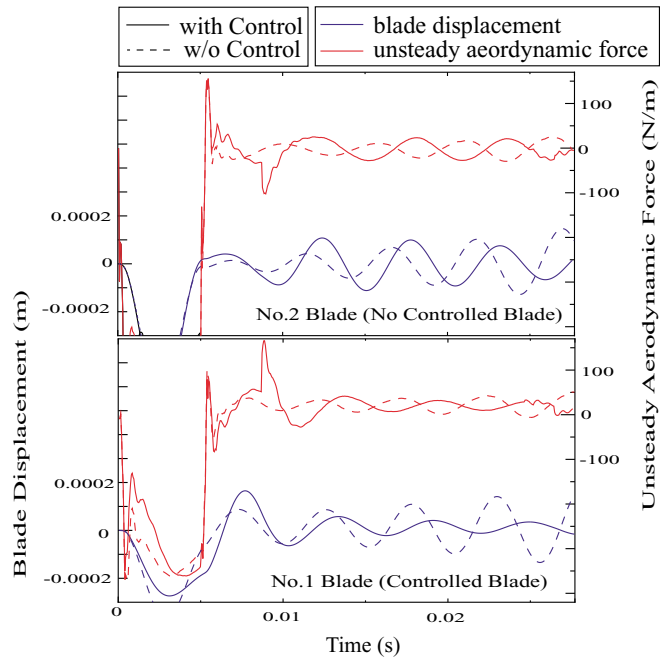


Figure 21 Time History of Blade Displacement and Unsteady Aerodynamic Force (Total energy rule used)

the behavior of the unsteady static pressure in downstream region of the passage shock, the static pressure data at the points shown in Fig. 17 were investigated in detail. The time histories of the static pressure at the point A on the blade surface, the point B, 1/2 of pitch distant from A, and the point C, 1/2 of pitch distant from A, are indicated and studied in the following figures.

Figures 18 and 19 show the time history of the static pressure at the three points above. The blade displacement is also indicated in the figures for the comparison of phase angle between the unsteady pressure and displacement. Figure 18 shows the results without control, while Fig. 19 shows those with control. In Fig. 18, the phase of static pressure is observed to advance compared with that of the blade displacement at all the three points A, B, and C. In this situation, the phase of the unsteady aerodynamic force induced by passage shock oscillation also advances, so that the aerodynamic force induced around the passage shock acts as an exciting force on the blade. The result well corresponds to the positive peak of aerodynamic work shown in Fig. 10. In the results with trailing edge oscillation shown in Fig. 19, on the contrary, the phase of the static pressure delays compared with that of the blade displacement. It means the unsteady aerodynamic force induced by the passage

shock oscillation acts as a damping force. As shown in Fig. 15, the peak of unsteady aerodynamic work on the blade surface diminishes in this case with control. The active trailing edge oscillation in the present study was thus revealed to change the phase of unsteady pressure, and the steep peak of unsteady aerodynamic work in the unstable side was thereby much alleviated.

### Flutter Suppression Analysis by Flow-Structure Coupled Method

From the previous results, it was revealed that the control by the trailing edge oscillation could change the unsteady aerodynamic force induced by passage shock oscillation from exciting to damping force. To confirm the effect of flutter suppression by the method, the flow-structure coupled analysis was performed on the case with control for the four flow-channels configuration shown in Fig. 20. In the computation, the initial velocity  $V_0=0.01C_0$  was given to No. 1 and No. 3 blades in the opposite directions, that is, the upward velocity was given to No. 1 blade while the downward one to No. 3 blade. On the other hand, the initial displacement was given to No. 2 and No. 4 blades. No. 2 blade was put on the initial position

of  $A=0.01C$ , while No.4 blade was put on the position of  $A=-0.01C$ . From the initial state, all blades started to oscillate with the inter blade phase angle of 90 degrees. The trailing edges of the No.1 and No.3 blades were oscillated with a phase advance of 90 degrees to the blade displacement. Figure 20 shows the computed time history of the unsteady aerodynamic force and the blade displacement in the case with control. The results without control are also shown for comparison. It is clearly indicated that the increase in the blade displacements is effectively suppressed by the control with trailing edge oscillation. The oscillation cycle of the controlled blade is seen to be longer than that of non-controlled blade probably because of the aerodynamic damping force acted on the control blade. The difference in vibration cycle should be another important factor for flutter suppression. The decrease in the displacement of non-controlled blade may be caused by the difference in the oscillation period, because the unsteady aerodynamic work distribution on the non-controlled blade, shown in Fig.15, is almost the same as that in the case without control.

Though the effectiveness of flutter suppression by trailing edge oscillation was confirmed in the previous results, it is necessary to verify that the control is effective if trailing edge vibration starts at a time independent of the initial situation. For this purpose, a rule using total energy of blade was adopted to detect the timing when the control should start, and the simulation by the flow-structure coupled method was performed.

The total energy of a blade,  $E$ , is defined as the sum of kinetic energy and structural energy of the blade;

$$E = \frac{1}{2} MV^2 + \frac{1}{2} Kh^2 \quad (8)$$

where,  $M$  is blade mass,  $V$  is blade velocity,  $K$  is spring constant of blade, and  $h$  is blade displacement.

The simulation was made for the same cascade as in Fig. 20. All blades were set stationary in the initial situation, and axial velocity disturbance was given as the Eq. (7) at the inlet boundary during one cycle of blade vibration. If the total energy of the blade,  $E$ , is larger than a constant value,  $E_0$ , the trailing edge of controlled blade is forced to oscillate.  $E_0$  is determined to be a value of the total energy when the blade amplitude is about 0.2% chord length. The trailing edges of the No.1 and No.3 blades are oscillated, and the total energy of the No.2 blade is observed. Figure 21 shows the computed time history of the blade displacement and the unsteady aerodynamic force. It is clearly shown that the increase in blade displacement is suppressed when the trailing edges start to oscillate at the time determined from the above rule.

## CONCLUSIONS

Possibility of active control on cascade flutter was numerically studied by use of a flow-structure coupled method. A cascade model operating in a transonic flow condition with passage shock waves was adopted for which the oscillation of shock wave played a dominant role for instability of blade vibration. In order to suppress the vibration, the trailing edge of a blade was actively oscillated in a flap-like manner. The active oscillation can be realized by application of some kind of smart structure with, for example, a piezo-electric device.

The conclusions are summarized as follows.

- 1.Cascade flutter phenomenon in the transonic flow with passage shock waves can be adequately simulated by the developed flow-structure coupled method.
- 2.In the present cascade model, the unsteady aerodynamic force induced by the passage shock oscillation was confirmed dominant for the blade vibration instability.
- 3.With the technique of trailing edge oscillation, the unsteady

aerodynamic force induced by the oscillatory movement of passage shock wave can be effectively changed from exciting force to damping one when the phase of trailing edge oscillation is adequately selected in comparison with that of the blade vibration displacement. The change in the unsteady aerodynamic force is caused by the change in the phase of passage shock oscillation due to the influence of trailing edge vibration.

- 4.In the case of unstable blade oscillation, it was confirmed that the increase in blade displacement was effectively suppressed by the present method of trailing edge vibration.

## REFERENCES

- [1] Epstein, A. H., Ffowcs Williams, J. E., and Greitzer, E. M., "Active Suppression of Aerodynamic Instabilities in Turbomachines", *Journal of Propulsion and Power*, Vol. 5, No.2, 1989, pp. 204-211.
- [2] Nagai, K. and Namba, M., "Effect of Acoustic Control on the Flutter Boundaries of Supersonic Cascade", *Unsteady Aerodynamics and Aeroelasticity of Turbomachines*, Fransson, T. H. ed., Kluwer Academic Publishers, 1998, pp.165-179.
- [3] Sun, X. , Jing, X. , and Zhao H. , "Control of Blade Flutter by Smart-Casing Treatment", *J.of Propulsion and Power*, Vol.17, No.2, 2001, pp248-255.
- [4] For Example, Scherer, L. B. , Martin, C. A. , West, M. , Florance, J. P. , Wiesman, C. D. , Burner, A. W. and Fleming, G. A. "DARPA/AFRL/ NASA Smart Wing Second Tunnel Test Results", *SPIE Vol.3674*, pp.249-259.
- [5] Kazawa, J. and Watanabe, T. , "Numerical Analysis toward Active Control of Cascade Flutter with Smart Structure", *AIAA Paper 2002-4079*.pp.1-9.
- [6] Obayashi,S and Kuwahara,K. : An approximate LU Factorization Method for the Compressible Navier-Stokes Equations, *Journal of Computational physics*, 1986, vol63, pp157-167
- [7] "Experimental Quiet Engine Program," contract No.NAS3-12430, March 1970.
- [8] Shibata, T. and Kaji, S. , "Role of Shock Structures in Transonic Fan Rotor Flutter", *Proc of the 8th International Symposium: Unsteady Aerodynamics of Turbomachines and Propellers*, Fransson, T. H. ed, Sept. 1997, pp.733-747.
- [9] Hanamura, Y., Tanaka, H., and Yamaguchi, K., "A Simplified Method to Measure Unsteady Forces Acting on the Vibrating Blades in Cascade", *Bulletin of JSME*, 1980, Vol.23, No.180, pp.880-887.